ARTICLES

Synthetic Macroporous Silicas with Multilamellar Structure

James G. C. Shen*

Department of Chemistry and Zettlemoyer Center for Surface Studies, 6 East Packer Avenue, Lehigh University, Bethlehem, Pennsylvania 18015

Received: December 16, 2002; In Final Form: October 17, 2003

We report a novel mixed-surfactant-based synthesis for growing new macroporous forms of silica. The dominant morphology is a fairly regular honeycomb-like construction with roughly 0.5−3-μm pores and 100−200-nm silica dividing walls. These walls consist of mesoscopic multilamellar structures. Interference optical microscopy observation and ^{23}Na and ^{13}C magic-angle spinning NMR diagnosed the single- and double-tailed surfactants with opposite charges on their headgroups, producing equilibrium vesicles spontaneously. A model that accounts for the architecture of the multilamellar silicas with macroporous morphologies involves the deposition of silica in the interfacial regions of contiguous assemblies of silicate−surfactant vesicles. Synthesizing shapes over μ-length scales provides new opportunities for understanding nature's biosilicification processes and potential uses where macroscopic form determines function, such as the separation, sensing, release, and catalysis of macro- and biomolecules.

Introduction

Organic matrix-mediated silicification in biological systems is responsible for the morphogenesis of spectacular forms of silica such as those found in diatoms and radiolaria.[1] The infinity of filigree patterns of the silica skeletons of these single-cell marine organisms, while delightful, has defied explanation in terms of form and function. Morphosynthesis engenders the idea of synthesizing shape over length scales found in nature's biominerals.[2] Like the morphogenesis of biomineral forms, morphosynthesis of inorganic materials invokes a biomimetic self-processing paradigm using preorganization, transcription, and replication construction stages of organics and inorganics in a hierarchical systems−synthesis pathway.[3] In this context, there is a notable trend of using supramolecular organic templates for the synthesis of inorganic materials with the complex form having structural features traversing micro- and mesoscopic dimensions.[4,5]

The recent investigations indicate that specific molecular interactions at organic−inorganic interfaces can result in the controlled nucleation and growth of inorganic crystals in the reaction media by several current routes. Route 1 involved the direct cocondensation of a cationic surfactant (S^+) with anionic inorganic species (I^-) to produce assembled ion pairs (S^+I^-). The synthesis of MCM-41 and MCM-48 are prime examples of this pathway.[6,7] In the charge-reversed situation (route 2), an anionic template (S^-) was used to direct the self-assembly of cationic inorganic species (I^+) through S^-I^+ ion pairs.[8] Routes 3 and 4 involved counterion (X^- or M^+)-mediated assemblies of surfactants and inorganic species of similar charge (assembled solution species $S^+X^-I^+$, where $X^- = Cl^-$ or Br^- or $S^-M^+I^-$, where $M^+ = Na^+$ or K^+).[9,10] Although the four pathways concluded successful synthesis of mesoporous inorganic materials, these conventional templating routes are not accessible for fabrication of macroporous materials that provide further understanding of biological silicification and for tailoring macroporous forms of silica in materials chemistry to separate colloids, bacteria, viruses, polymers, and biomolecules. In part, this is because organic molecular micelles cannot fit the magnitude of a macroscopic structure to template macrocavities of inorganic materials. To take small organic molecules and micellar-based patterning of silica beyond the micro- and mesoscale, based on foams, vesicles, or microemulsions, often generating boundary surfaces and imprints for the sculpting of complex forms in inorganic materials,[11] one expects to find a new way of using vesicles to shape and imprint macroscopic decorations into silica.

A model for the growth of honeycomb-like macrostructured forms of silica must take into account recent studies of the phase behavior and equilibrium aggregate morphology of aqueous mixtures of oppositely charged cationic and anionic surfactants.[12−14] Pertinent mixtures of oppositely charged cations and anionic surfactants can create stable narrow dispersions of vesicles under mild aqueous conditions.[12−14] The didodecyldimethylammonium bromide (DDAB) cation and sodium dodecyl sulfate (SDS) anion surfactant pairs behave as triple-tailed zwitterionic surfactants, which spontaneously produce vesicles in a narrow range of compositions without mechanical or chemical perturbations to the system (e.g., detergent dialysis).[13] For the domain of such vesicles of DDAB, SDS, and water, the phase diagram provides a good starting point for the synthesis of silicate macrostructure. The choice of the DDAB/SDS/H_2O ratio provides considerable scope for tailoring the surface charge, curvature, and permeability properties of the vesicles.[13] The diversity provides control mechanisms over their

* Present address: Specialty Minerals, 9 Highland Avenue, Bethlehem, PA 18017-9482. E-mail: jgcshen50@hotmail.com.

10.1021/jp0277412 CCC: $27.50
Published on Web 12/05/2003

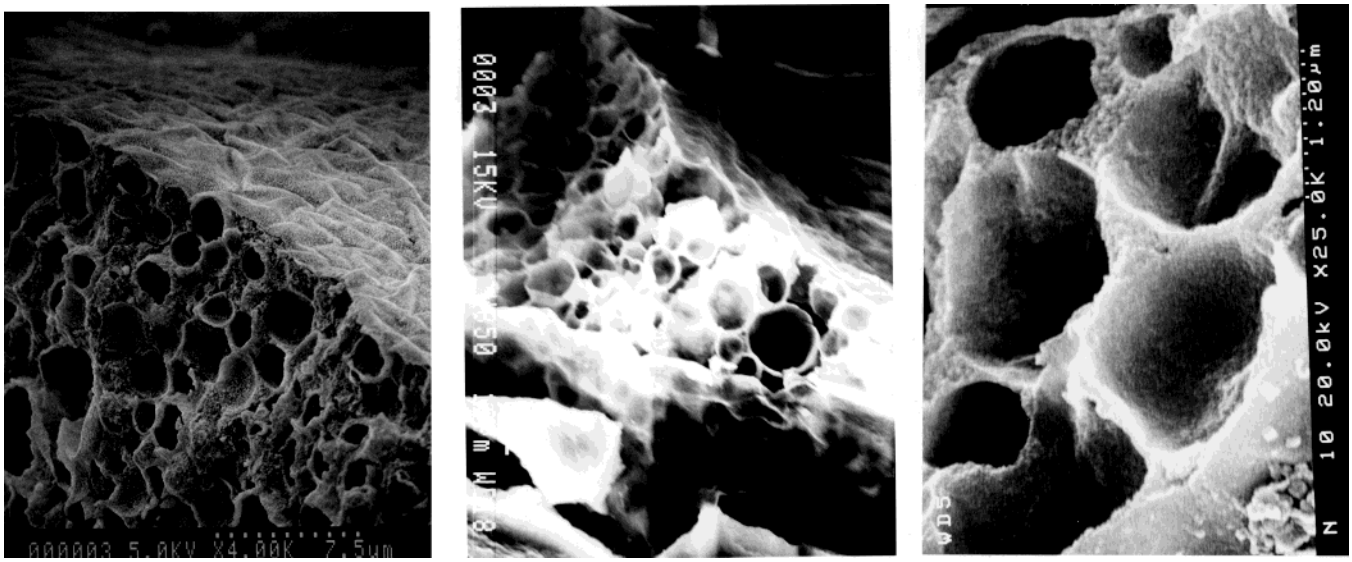

Figure 1. SEM image of the as-synthesized vesicle-templated sample with initial molar ratio of 2778 H_2O/1.3 TA/2.5 DDAB/0.5 SDS/10.0 TEOS depicting a honeycomb-like macrostructure. (a) and (b) Bulk with honeycomb with roughly 0.5−3-μm pores. (c) 100−200-nm silica dividing walls.

size, dispersion and aggregation properties, and ultimately the transcription of this vesicle information into patterned silica replicas.

Experimental Section

Synthesis. The meso-multilamellar macroporous forms of silica were synthesized by using a mixture of didodecyldimethylammonium bromide (DDAB, $(CH_3(CH_2)_{11})_2N(CH_3)_2Br$, Alldrich) cation and sodium dodecyl sulfate (SDS, $CH_3(CH_2)_{11}SO_3Na$, Aldrich) anion surfactants as structure-directing agents and tetraethoxysilan (TEOS, $Si((C_2H_5O)_4$, Aldrich) as a silica source reagent under acidic conditions. A series of typical preparations was achieved using the following reactant mole ratio, 2778 H_2O/1.3 TA/2.5 DDAB/0.5 SDS/9−15 TEOS, where DDAB and SDS reached their CMC (critical micelle concentration)[13] and TA is tartaric acid. Another series of preparations was carried out employing the same mole ratio reagents but with HCl instead of tartaric acid. The DDAB was mixed with SDS in the acidic aqueous solution with vigorous stirring at room temperature for 30 min. Gelation occurred immediately, yielding a vesicle-like viscous suspension. TEOS was added to the suspension under continuous stirring for 30 min. The resultant mixture was placed into a sonics (Cole-Parmer 8891) for another 30 min sonication, then transferred into a polypropylene bottle, and heated at 80 °C for 72 h without stirring. After the solution cooled to room temperature, the solid product was recovered by filtration, washed with water, and dried in ambient atmosphere, yielding an as-synthesized sample. The resulting powders were calcined at 400 °C for 3 h to remove the organic surfactants.

Analyses. Powder X-ray diffraction (PXRD) patterns were obtained using a Siemens D-500 wide-angle X-ray diffractometer with Cu Kα radiation. The sample morphology was determined by scanning electron microscopy (SEM) with a Hitachi S4500 field emission microscope at an accelerating voltage of 20 kV. Transmission electron microscopy (TEM) images were taken on a Philips 430 microscope operating at 100 kV with a tungsten filament. The samples for TEM were prepared by epoxy embedding and microtomed into ∼300-Å sections. Differential interference optical microscope (IOM) images of the samples were recorded on a Nikon optical microscopy (model OPTIPHOTO2-POL).

^{29}Si solid-state MAS NMR spectra were recorded on a Chemagnetics CMX-500 spectrometer operating at a ^{29}Si resonance frequency of 59.71 MHz under MAS conditions of 3.0 kHz at room temperature; $\pi/2$ pulse lengths of 6−7 μs were used to acquire one pulse. ^{29}Si spectra resulted from 100−300 signal-averaged accumulations, employing a 300-s repetition delay between each scan. The ^{29}Si MAS spectra are referenced to tetramethylsilane, $Si(CH_3)_4$. ^{23}Na solid-state MAS NMR experiments were carried out at 11.7 T on a Chemagnetics a CMX-500 spectrometer at room temperature. The spinning speed was 5.0 kHz. A total of 10,000−30,000 acquisitions were accumulated in each experiment with a pulse length of 4 μs. The spectra were zero filled to 2K data points, with application of 200-Hz Lorentzian broadening. The external reference was a 0.1 M NaCl solution. ^{13}C solid-state MAS NMR spectra were also recorded with a Chemagnetics CMX-500 spectrometer operating at 75.47 MHz. The measurements were carried out at room temperature using 3.5-μs pulse lengths, a 3.0-kHz spinning speed, and a 60-s empirically determined relaxation delay. The ^{13}C MAS spectra are referenced to *N*-acetyl glycine.

Results and Discussion

The Characterization of the Silicate−Surfactant Phase by SEM, TEM, PXRD, and ^{29}Si Solid-State MAS NMR. The phase separation in the polypropylene bottle at 80 °C, in the present experiment, can be observed through optical microscopy. A relatively large volume of the H_2O-rich isotropic phase was present, containing soluble silicate and surfactants. More viscous silicate−surfactant-rich phases are comprised of aggregates that can organize into liquid crystalline arrays with long-range order.[11] The two phases establish an equilibrium at 80 °C. This is in agreement with the work of Firouzi et al. that demonstrates the two-phase features of the multicomponent silicate−surfactant mixtures through a L_α (L designates lamellar phase, subscript α designates the anisotropic liquidlike mobility of the alkyl surfactant chain in the silicate−surfactant mesophase) deuterium NMR powder pattern.[11,15] After a 72 h reaction at 80 °C, the silicate−surfactant-rich phase precipitated onto the bottle bottom.

SEM images of the as-synthesized sample show that the majority of silica consists of honeycomb-like morphologies with roughly 0.5−3.0-μm pores and 100−200-nm silica dividing walls (Figure 1). TEM images of microtomed sections of the

Figure 2. TEM image of the as-synthesized vesicle-templated sample with initial molar ratio of 2778 H_2O/1.3 TA/2.5 DDAB/0.5 SDS/10.0 TEOS showing that the silica walls of the macrostructure are a multilamellar structure with ~3-nm interlamellar spaces.

as-synthesized materials show that the silica walls are mesoscopic multilamellar structures with ~3-nm interlamellar spaces (Figure 2). The PXRD pattern for the as-synthesized sample confirms the glassy dense-packed nature of the silica wall regions (Figure 3). The first two intense (00*l*) peaks ($l = 1, 2$) provide an indication of the mesolamellar silica wall with an interlamellar spacing of 32.8 Å, and the phase gives no higher-angle peaks (Figure 3B). Such interlamellar spacing formation was widely studied, which resulted from templating of the surfactants-assembled double layer.[3−10] The PXRD showed another sample synthesized in a pH = 0.6 acidic condition with an interlamellar spacing of 29.4 Å and relatively lower intensity. The low pH in the synthetic matrixes resulted in the decrease of interlamellar spaces, as represented by the PXRD patterns ($\Delta d = 3.3$ Å in parts A and B of Figure 3). This may be ascribed to the fact that the low-pH matrixes promote hydrogen-bond formation between the silicas and surfactant headgroups and slow silicate polymerization.[4] After the surfactants were removed by calcination at 400 °C, the silica wall of the resulting material maintained the mesolamellar structure.

^{29}Si MAS NMR data (Figure 4) were used to determine the degree of condensation of silicate in the as-synthesized materials. The resonance peak at 102.7 ppm is consistent with Q_3 (SiO_3-(OH)), while the resonance signal at 112.4 ppm corresponds with Q_4 (SiO_4).[9] The concentration of silanol groups is measured by the ratio Q_4/Q_3. From the areas of the Q_4 and Q_3 signals, the number of ^{29}Si of the type $(SiO)_3{\equiv}Si{-}O{-}Si{\equiv}$ and $(SiO)_3{\equiv}Si{-}OH$ can be determined, respectively. The estimated error in the values of Q_4 and Q_3 is about ±5% of their value. The ^{29}Si NMR spectra of the mesolamellar structural wall of the macroporous morphology silica showed a Q_4/Q_3 ratio of ~78/22 (Figure 4). On the other hand, the synthesized silica materials in HCl conditions exhibited a Q_4/Q_3 ratio of ~65/35. These ^{29}Si NMR data are in agreement with studies of pH influence

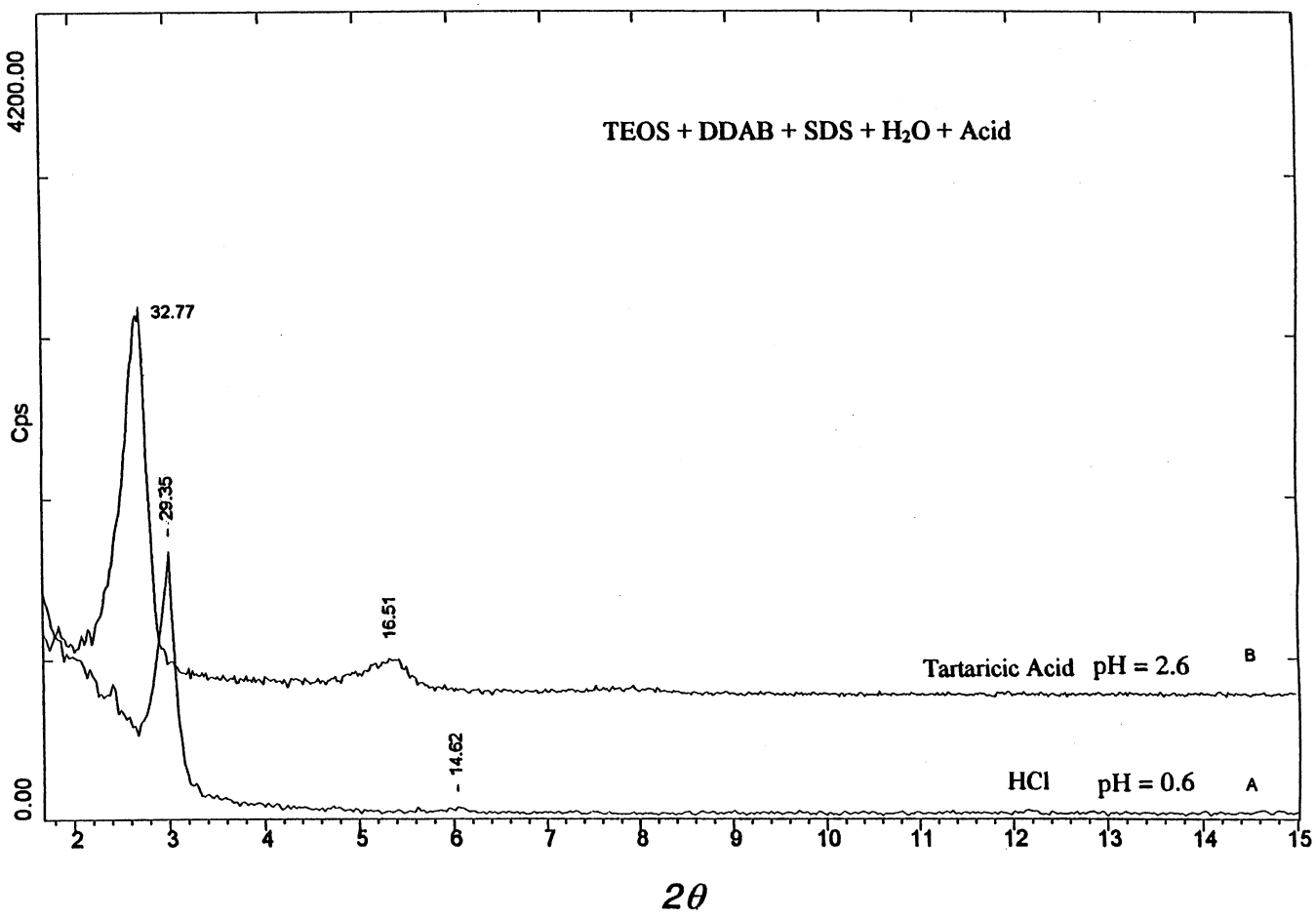

Figure 3. The PXRD pattern in the range $0° < 2\theta < 15°$ of the as-synthesized vesicle-templated samples with initial molar ratio of 2778 H_2O/1.3 TA−HCl/2.5 DDAB/0.5 SDS/10.0 TEOS.

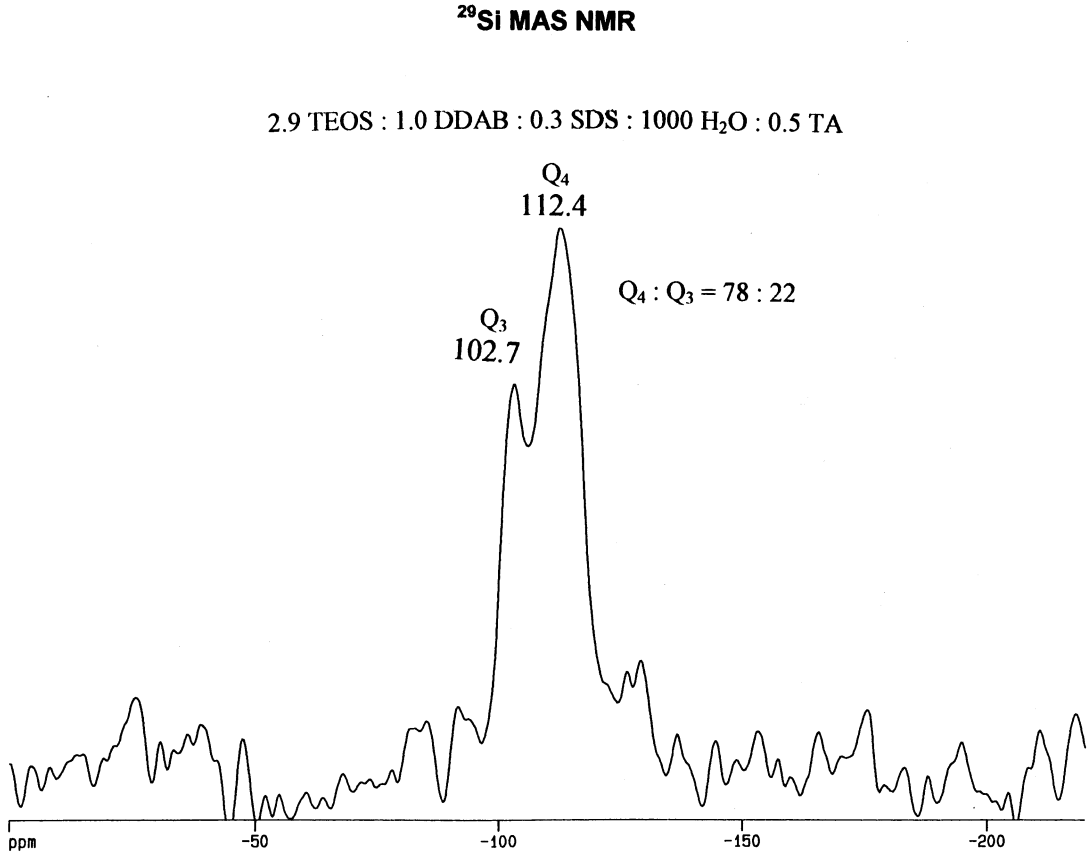

Figure 4. ^{29}Si solid-state MAS NMR spectra of the as-synthesized sample.

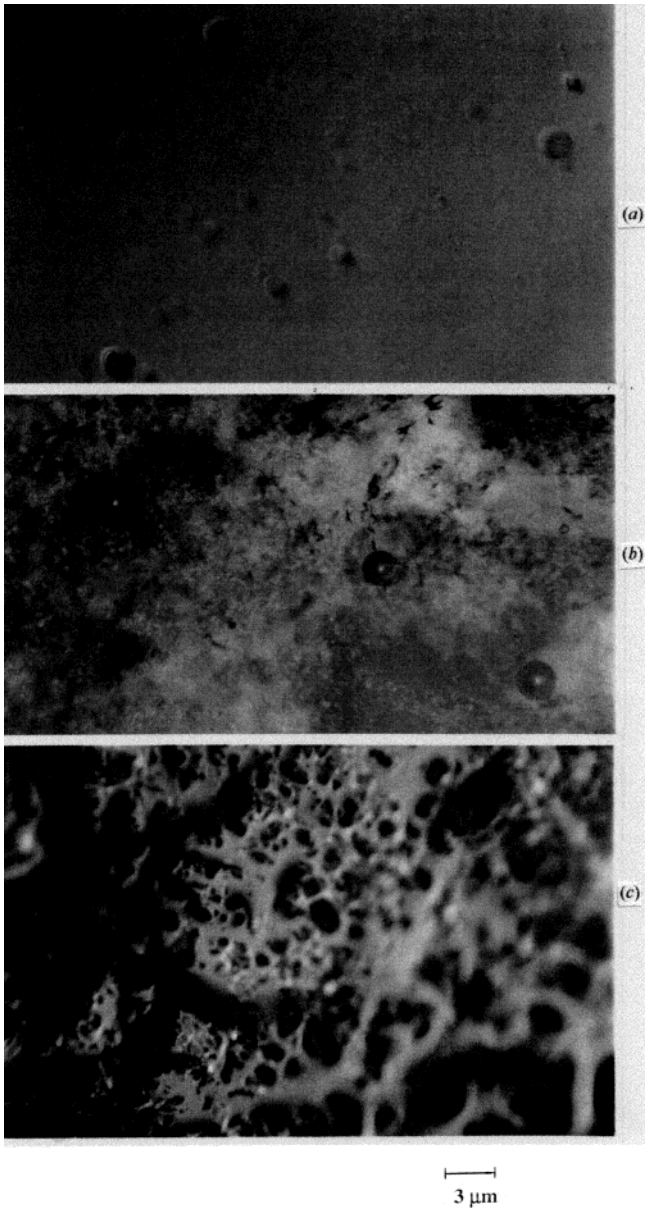

Figure 5. IOM images of the DDAB/SDS/H_2O/TEOS/TA system with the same molar ratio as in the as-synthesized sample during the heating process. (a) View of DDAB/SDS/H_2O at room temperature, (b) view of DDAB/SDS/H_2O/TEOS/TA after aging at room temperature overnight, and (c) view of DDAB/SDS/H_2O/TEOS/TA annealing at 60 °C.

upon silicate condensation, where silicate polymerization is slowed under pH < 2 conditions.[1]

The principal criteria for the formation of an inorganic−organic phase are that the inorganic component must be capable of forming flexible polyionic species, that extensive polymerization of the inorganic component must be possible, and that charge-density matching between the surfactant and inorganic species has to occur.[11,15] Chmelka et al. claimed that silicate polymerized in a pH = 2−7 of the matrix at room temperature into double four-ring (D4R) units ($Si_8O_{20}^{8-}$) and double three-ring (D3R) units ($Si_6O_{15}^{6-}$). These possess little energetic advantage over other monovalent anions (such as Br^-) competing for access to the DDA^+ cationic headgroup to form thermodynamically stable silicate−surfactant arrays.[11] An attractive van der Waals-type interaggregate force can be present among the highly polarizable and mobile silicate oligomers in the diffusive double layer surrounding the aggregates and dominate repulsive interactions in the oligometric aggregation.[11,16] The highly charged double-ring silicate oligomers interact with the cationic surfactant headgroups through hydrogen bonds and thereby induce the self-assembly of a silicate−surfactant phase.[4b] After aging in the matrix at 80 °C, D_4R and D_3R oligomers condensed into Q_4/Q_3 silicates between double-layer surfactant arrays, as shown in Figure 4.

The Characterization of Silicate−Surfactant Phase by in situ Optical Microscopy. In IOM, characteristic optical patterns from different defect structures lead to mesophase-special textures that can be used to identify different phase morphologies.[11] The ternary DDAB/SDS/H_2O phase was measured immediately after loading the sample into a thin flat capillary that reflected alignment of the mesophase produced by shear flow during the loading process,[17] using the in situ temperature program Nikon optical microscopy. At room temperature, the surfactant phase (DDAB/SDS/H_2O) showed 1.0−3.0 μm diameter vesicle features (Figure 5a). After aging at room temperature overnight, a vesicle-like texture corresponding to silicate−surfactant phase (DDABSDS/H_2O/TEOS/TA) was also observed in Figure 5b. By heating the silicate−surfactant sample to 60 °C, the vesicle-like optical pattern developed, as shown in Figure 5c, and the honeycomb-like macroporous architecture appeared. The vesicle texture is the precursor characteristic of the macroporous morphology of the resulting materials,[17,18] which correspond to the SEM patterns in Figure 1. In addition, an existing precipitation phenomenon was observed in the IOM, which resulted from the strong interaction of cooperative binding of the surfactant−silicate micellar aggregates that need to precipitate into a macrophase from dilute solution.[11] Preferential polymerization of silicates in the region of the interface, together with the doubl-layer control in the interlamellar spacing of walls, would be responsible for the high regularity of the surfactant−silicate mesostructures.[11] These IOM pictures provide corroborative verification of the vesicle texture and demonstrate a processing advantage of preserving vesicle properties prior to the polymerization of silicate species in the silicate−surfactant mesophase.

The Confirmation of Vesicle Formation by ^{23}Na and ^{13}C MAS NMR. *^{23}Na MAS NMR Study*. To obtain more insight into the mechanism of macroporous silica formation, especially into the vesicle templating, ^{23}Na ($I = {}^3/_2$) MAS NMR spectra were recorded. Figure 6, curve A shows the ^{23}Na MAS NMR spectrum of powder SDS, which indicates a broad peak at −14.5 ppm, consistent with the ^{23}Na resonance of anionic SDS. Such a broad resonance signal is attributed to a relatively large charge asymmetry and large second-order quadrupolar broadening effect in Na^+ sites of the powder SDS.[19,20] A synthetic intermediate texture with the same composition of 2778 H_2O/1.3 TA/2.5 DDAB/0.5 SDS as in the as-synthesized sample was prepared without filtration and washing and dried in ambient atmosphere, which shows a sharp ^{23}Na resonance at 5.9 ppm (Figure 6, curve B). This ^{23}Na resonance peak shifted downfield 20.4 ppm from the ^{23}Na resonance of the anionic SDS powder. In the intermediate texture, the cationic DDAB attached to anionic SDS surfactant to form a $DDAB^-{-}^+SDS$ ion pair and changed the chemical environment around Na^+ sites. Therefore, the Na^+ resonance signal of the matrix changed to a sharp Gaussian peak.[19−21] The downfield shift (−14.5 → 5.9 ppm) is assigned to an incorporation of an isotropic chemical shift, δ_{cs}, related to the charge density around Na^+ sites, and an isotropic second-order quadrupolar shift, $\delta_{Q,iso}$, related to the asymmetry parameter η and the quadrupole coupling constant (QCC or e^2qQ/h) of the Na^+ sites in the intermediate texture.[19−21] The ^{23}Na signal in the as-synthesized sample is shifted downfield

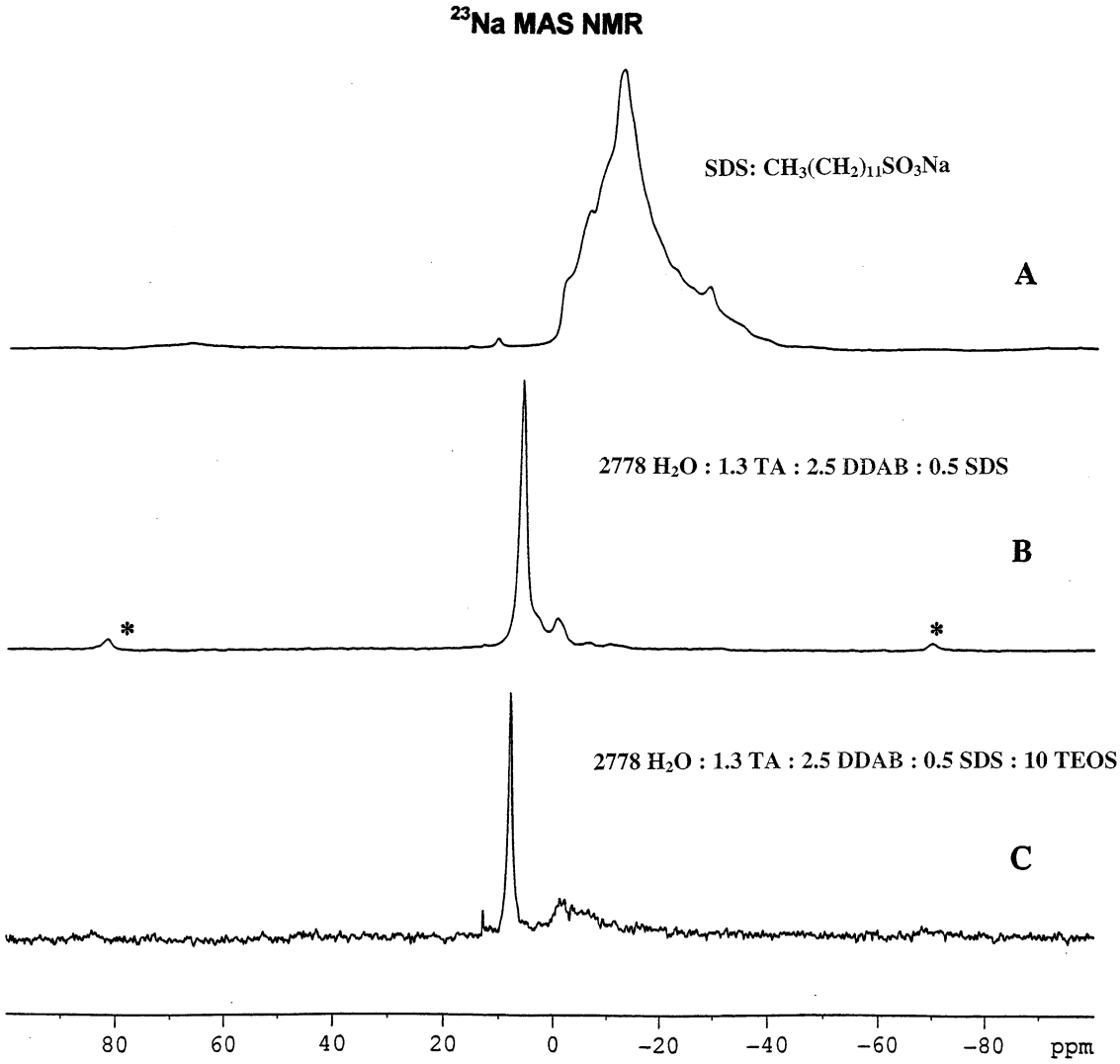

Figure 6. ^{23}Na solid-state MAS NMR of (a) powder SDS, (b) the DDAB/SDS/H_2O/TEOS/TA system with the same molar ratio as in the as-synthesized sample, and (c) the as-synthesized sample.

to 7.8 ppm (Figure 6, curve C) from both the SDS powder (−14.5 ppm in Figure 6, curve A) and the intermediate texture (5.9 ppm in Figure 6, curve B). The 1.9 ppm downfield shift of ^{23}Na resonance peaks in curves B and C of Figure 6 is ascribed to the chemical environment further changing around Na^+, such as a reduction of electron densities and QQC in Na^+ cation sites and an increase of the asymmetry (η).[19−21] This change in the chemical environment originates from oligomeric silicate (Q_4/Q_3) interactions with units of DDAB coupled to SDS in the resulting macroporous material.[15] Specially, silicate polymerization occurred between the double layer of SDS-coupling DDAB.[11] The DDAB-coupling SDS is diagnostic for vesicle formation. Present observation of ^{23}Na resonance shifts provide evidence of DDAB-coupling SDS and oligomeric silicate, which result in vesicle texture occurring in the matrix. Under present experimental circumstances, the flexible surfactant chains of units of DDAB coupled to SDS in the hydrophobic region of an aggregate become rigid; the surfactant molecules can no longer pack into curved structures. Thus the aggregates become insoluble, resulting in crystallization of the pure DDAB−SDS pair with its associated silicate species,[22] and the resulting lamellar silica materials are a replica of the layered silicate−surfactant mesophase. The vesicles are responsible for the growth of the honeycomb-like silica architecture.

^{13}C MAS NMR Study. Figure 7, curve A shows the ^{13}C MAS NMR spectra of the DDAB powder. A couple of sharp peaks shown at 49.5 and 48.2 ppm are ascribed to ^{13}C resonance of the dimethyl group in the DDAB.[23,24] Another doublet of broad peaks at 65.5 and 61.8 ppm are assigned to ^{13}C resonance of two α carbons of the dodecyl chains in the DDAB.[23,24] The pure SDS powder presents a sharp ^{13}C resonance signal at 68.9 ppm, which is assigned to the α carbon of the dodecyl chain in the SDS[23,24] (Figure 7, curve B). The intermediate texture contained the same molar ratio and synthetic processes as those in Figure 6B and exhibits the ^{13}C MAS NMR signals in Figure 7, curve C. Except for the two coupled peaks at 49.5, 48.2, 65.8, and 61.8 ppm, five new peaks are observed at 50.8, 51.3, 59.8, 60.4, and 67.1 ppm. The peaks at 50.8 and 51.3 ppm are attributed to the ^{13}C resonance of the dimethyl in a unit of DDAB coupled to SDS that is a necessary condition for the vesicle textures formation. The downfield shifts, $\delta = 2.6$ ppm (48.2 → 50.8 in parts A to C in Figure 7) and $\delta = 1.8$ ppm (49.5 → 51.3 in parts A to C in Figure 7) are due to the deshielding effect of carbon in the dimethyl of DDAB coupled to SDS, corresponding with electron density decrease in the carbon of the dimethyl.[24] Such electronic deshielding is considered to result from a fractional electron transferred from DDAB to the SDS in their coupled unit. This is consistent with

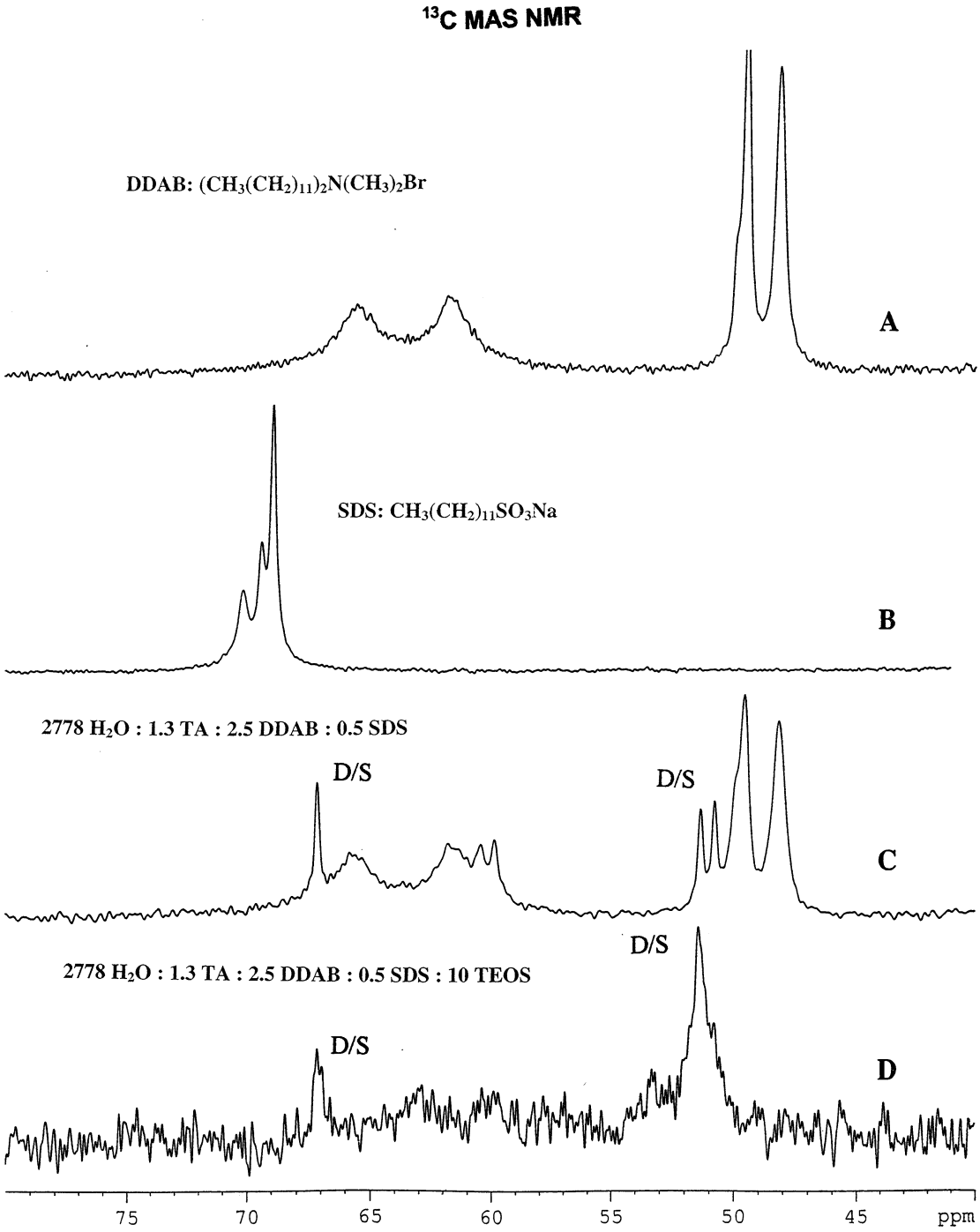

Figure 7. ^{13}C solid-state MAS NMR of (a) powder DDAB, (b) powder SDS, (c) the DDAB/SDS/H_2O/TEOS/TA system with the same molar ratio as in the as-synthesized sample, and (d) the as-synthesized sample.

inference that the Na of SDS absorbs the electron density of the carbon in the dimethyl in the unit of DDAB and SDS, which results in the increase of the δ value. The peak at 67.1 ppm in Figure 7, curve C is assigned to ^{13}C resonance of the α carbon in the unit of SDS coupled to DDAB. The δ decrease from 68.9 ppm in Figure 7, curve B to 67.1 ppm in Figure 7, curve C, is consistent with the proposal that DDAB donated electron density to the α carbon of the SDS, resulting in the electronic shielding of the α carbon and decreased δ value. The several ^{13}C peaks in Figure 7, curve C provide an indication that the unit phase of DDAB coupled to SDS and DDAB's own phase were involved in the intermediate textures. This is in agreement with the synthetic formula that 2.0 M excess DDAB existed in a phase of 0.5 M SDS coupled to 0.5 M DDAB (see Experimental Section). Figure 7, curve D shows the ^{13}C MAS NMR spectra of the as-synthesized sample that correspond to macroporous SEM images (Figure 1). The single peak at 51.4 ppm is due to the ^{13}C resonance signal of the α carbon of the dimethyl in the DDAB, while another peak at 67.1 ppm is assigned to the ^{13}C resonance for the α carbon of the SDS in the vesicle texture.[23,24] The disappearance of the 48.2 and 49.5 ppm peaks of the α carbon of the dimethyl in the DDAB phase imply full removal of excess DDAB phase by filtration. The single ^{13}C signal at 51.4 ppm suggests that two α carbons of dimethyl in the unit of DDAB coupled to SDS were located in an equivalent chemical environment. Consequently, ^{13}C reso-

nance shifts indicated the existence of units of DDAB coupled to SDS in the resulting sample that further proves the occurrence of vesicle textures, which transcribe their character into the macroporous silica replica.

The presence of vesicles in the surfactant precursor solution, which promotes the existence of long-range van der Waals forces, appears to be an important prerequisite for self-assembly to occur.[11,15] The consequence of such prevailing attractive interactions is that the aggregates self-assemble and phase separation is induced, whereby one or more concentrated silicate−surfactant-rich phase adopts morphologies (see Figures 1 and 5) that minimize the total Gibbs free energy and establish a new equilibrium condition.[11] The attractive interaggregate interactions are dominant, further suggesting that the mean aggregate shape for the L_α silicate−surfactant phase should be lamellar,[11,15] which is transcribed into the resulting mesolamellar silica materials as indicated by PXRD and TEM measurements.

In the case of mesoporous forms of silica, the general consensus is that they form through the coassembly of surfactant−silicate micellar aggregates that undergo condensation−polymerization into a silica replica.[6] One can propose that in order to move up the hierarchical ladder of scale, the mode of formation of silica with a macroscopic honeycomb-like architecture likely involves collective interactions between silicate building blocks and DDAB/SDS-based vesicle solution species. Deposition of silica probably occurs in the interfacial regions of contiguous aggregations of silicate−surfactant vesicles to create a micron scale patterned silica replica. This is reasonable as the DDAB/SDS/silicate vesicle assembly process can be directly observed in the optical microscope.

Conclusion

The paper demonstrates the honeycomb-like macroporous morphologies with dividing silica walls of mesolamellar structure. The DDAB cation and SDS anion surfactant pairs in certain ratios spontaneously produce vesicles that were proved by IOM observation and ^{23}Na and ^{13}C MAS NMR characterization. Such vesicles direct the morphogenesis of the honeycomb-like macroporous silica while self-assembly surfactant micelles template the formation of mesolamellar dividing silica walls. The vesicle-directing model may involve collective interactions between silicate building blocks and oppositely charged DDAB/SDS vesicle micelle species and deposition of silica in the interfacial regions of contiguous aggregations of silicate−surfactant vesicles.

The dual-templating micelle−vesicle synthesis pathway yields the new class of meso-macroporous materials which could provide access generally to a wide range of micro- to macroporous inorganic−organic composite materials.

References and Notes

(1) *Silicon and Siliceous Structures in Biological Systems*; Simpson, T. L., Volcani, B. E., Eds.; Springer-Verlag: New York, 1981.
(2) Ozin, G. A. *Acc. Chem Res*. **1997**, *30*, 17.
(3) Mann, S.; Ozin, G. A. *Nature* **1996**, *382*, 313−318.
(4) (a) Oliver, S.; Kuperman, A.; Coombs, N.; Lough, A.; Ozin, G. A. *Nature* **1995**, *378*, 47−50. (b) Boissière, C.; Martines, M. A. U.; Tokumoto, M.; Larbot, A.; Frouzet, E. *Chem. Mater*. **2003**, *15*, 509.
(5) Walsh, D.; Mann, S. *Nature* **1995**, *377*, 320−323.
(6) Kresge, C. T.; Leonowicz, M. E.; Roth, W. J.; Vartuli, J. C.; Beck, J. S. *Nature* **1992**, *359*, 710−12.
(7) Beck, J. S.; Vartuli, J. C.; Roth, W. J.; Leonowicz, M. E.; Kresge, C. T.; Schmitt, K. D.; Chu, C. T. W.; Olson, D. H.; Sheppard, E. W.; McCullen, S. B.; Higgins, J. B.; Schlenker, J. L. *J. Am. Chem. Soc*. **1992**, *114*, 10834.
(8) Monnier, A.; Schüth, F.; Huo, Q.; Kumar, D.; Margolese, D.; Maxwell, R. S.; Stucky, G. D.; Krishnamurty, M.; Petroff, P.; Firouzi, A.; Janicke, M.; Chmelka, B. F. *Science* **1993**, *261*, 1299.
(9) Huo, Q.; Margolese, D. I.; Clesla, U.; Feng, P.; Gler, T. E.; Sleger, P.; Leon, R.; Petron, P. M.; Schuth, F.; Stucky, G. D. *Nature* **1994**, *368*, 317.
(10) Tanev, P. T.; Chibwe, M.; Pinnavaia, T. J. *Nature* **1994**, *368*, 321.
(11) Firouzi, A.; Atef, F.; Oertli, A. G.; Stucky, G. D.; Chmelka, B. F. *J. Am. Chem. Soc*. **1997**, *119*, 3596.
(12) Kaler, E. W.; Kamalalaka Murthy, A.; Rodriguez, B. E.; Zasadzinski, J. A. N. *Science* **1989**, *245*, 1371−74.
(13) Kondo, Y.; Uchiyama, H.; Yoshino, N.; Nishiyama, K.; Abe, M. *Langmuir* **1995**, *11*, 2380.
(14) Yatcilla, M. T.; Herrington, K. L.; Brasher, L. L.; Kaler, E. W.; Chiruvolu, S.; Zasadzinski, J. A. N. *J. Phys. Chem*. **1996**, *100*, 5874.
(15) Firouzi, A.; Kumar, D.; Bull, L. M.; Besier, T.; Sieger, P.; Huo, Q.; Walker, S. A.; Zasadzinski, J. A.; Glinka, C.; Nicol, J.; Margolese, D.; Stucky, G. D.; Chmelka, B. F. *Science* **1995**, *267*, 1138.
(16) Firouzi, A.; Stucky, G. D.; Chmelka, B. F. *Synthesis of Microporous Materials*; Occelli, M. L., Kessler, H., Eds.; Marcel Dekker: New York, 1996; pp 370−389.
(17) Miller, C. A.; Ghosh, O.; Benton, W. *J. Colloid Surf.* **1986**, *19*, 197.
(18) Rosevear, F. B. *J. Soc. Cosmet. Chem*. **1968**, *19*, 581.
(19) Shen, J. G. C. *J. Phys. Chem. B* **2001**, *105*, 2336.
(20) Hunger, M.; Engelhardt, G.; Koller, H.; Weitkamp, J. *Solid State Nucl. Magn. Reson*. **1993**, *2*, 111.
(21) Lim, K. H.; Grey, C. P. *J. Am. Chem. Soc*. **2000**, *122*, 9768.
(22) Groenen, E. J. J.; Emeis, C. A.; van den Berg, J. P.; de Jong-Versloot, P. C. *Zeolites* **1987**, *6*, 474.
(23) *Hand Book of NMR Spectroscopy and Applications*; Evans, E. A., Warrell, D. C., Elvidge, J. A., Jones, J. R., Eds.; Wiley & Sons: New York, 1985.
(24) Kemp, W. *NMR in Chemistry*; Macmillan Publishing Co.: New York, 1988.